ISSN (Online) 2394-6849

International Journal of Engineering Research in Electronics and Communication Engineering (IJERECE)
Vol 4, Issue 12, December 2017

# Computer Aided Brain Tumor Localization and Tumor Growth Model Generation based on Machine Learning Techniques

[1] Chitra K, [2] Ahila A
[1] Department of ECE, Keelavallanadu, Thoothukudi Infant Jesus College of Engineering
[2] Department of ECE Infant Jesus College of Engineering Keelavallanadu, Thoothukudi

***Abstract:*** **- In this paper, we propose a proof of concept for the automatic planning of personalized radiotherapy for brain tumors. A computational model of brain tumor growth is combined with an exponential cell survival model to describe the effect of radiotherapy. The model is personalized with the magnetic resonance images (MRIs) of a given patient. It takes into account the uncertainty in the model parameters, together with the uncertainty in the MRI segmentations. The computed probability distribution over tumor cell densities, together with the cell survival model, is used to define the prescription dose distribution, which is the basis for subsequent Intensity Modulated Radiation Therapy (IMRT) planning. Depending on the clinical data available first, we include the uncertainty in the segmentation process. We show how our method allows the user to compute a patient specific radiotherapy planning conformal to the tumor growth. The presented approach and its proof of concept may help in the future to better target the tumor and spare organs at risk.**

## I. INTRODUCTION

Brain tumor is a mass or collection of abnormal cells in brain. Brain tumor arises due to abnormal growth of cells that have proliferated in an uncontrolled manner. When normal cells grow old and die or get damaged cell death. Some mutation occur in cellular DNA that give rise to more cells that all contain abnormal DNA. The accumulating cells from the mass is called growth or tumor. A brain tumor is an abnormal growth of tissue in the brain or central spine that can disrupt proper brain function. The cause of most brain tumors is unknown, it may occur due to radiation like ultraviolet, mobile phones, genetic mutation, heriditatory reasons but the evidence is not clear several research studies have claimed that diseases caused due to impaired gene function like neurofibromatosis and Li-Fraumeni syndrome also put at high risk of brain tumors. Although brain tumors can occur at any age, elderly people are known to be at a high risk of suffering from this disease. In the year 2006 at TATA Memorial Hospital in Mumbai, India 372 people were diagnosed with Brain and Central Nervous System Tumors, out of which 250 (67%) were males and 122 (33%) were females. A total of 1,529,560 new cancer cases and 569,490 deaths from cancer are projected to occur in the United States in 2010. Overall cancer incidence rates decreased in the most recent time period in both men (1.3% per year from 2000 to 2006) and women (0.5% per year from 1998 to 2006), largely due to decreases in the 3 major cancer sites in men (lung, prostate, and colon and rectum [colorectum]) and 2 major cancer sites in women (breast and colorectum). The reduction in the overall cancer death rates translates to the avoidance of approximately 767,000 deaths from cancer over the 16-year period The most effective and common tool for diagnosing a brain tumor is the use of a Magnetic Resonance Imaging (MRI) scan, although Computed Tomography (CT or CAT) scans are also used. A Positron Emission Tomography (PET) scan is used at first to find out more about a tumor while a patient is receiving treatment or if the tumor comes back after treatment. A variety of therapies are used to treat brain tumors. The type of treatment recommended depends on the size and type of the tumor, its growth rate, brain location, and the general health of the patient. Treatment options include surgery, radiation therapy, chemotherapy, targeted biological agents, or a combination of these. Surgical resection is generally the first treatment recommendation to reduce pressure in the brain rapidly. In the past two decades, researchers have developed new techniques of delivering radiation that target the brain tumor while protecting nearby healthy tissues. These treatments include brachytherapy, Intensity Modulated Radiation Therapy (IMRT) and radiosurgery.

Radiation therapy may be advised for tumors that are sensitive to this treatment. Conventional radiation therapy uses external beams of x-rays, gamma rays or protons aimed at the tumor to kill cancer cells and shrink brain tumors. The

ISSN (Online) 2394-6849

International Journal of Engineering Research in Electronics and Communication Engineering (IJERECE)
Vol 4, Issue 12, December 2017

therapy is usually given over a period of several weeks. Whole brain radiation therapy is an option in the case of multiple tumors or tumors that cannot be easily targeted with focal treatment. Types of radiation therapy include:
An advanced mode of high-precision radiotherapy that utilizes computer-controlled x-ray accelerators to deliver precise radiation doses to a malignant tumor or specific areas within the tumor. The radiation dose is designed to conform to the three-dimensional (3-D) shape of the tumor by modulating or controlling the intensity of the radiation beam to focus a higher radiation dose to the tumor while minimizing radiation exposure to healthy cells. A highly precise form of radiation therapy that directs narrow beams of radiation to the tumor from different angles. For this procedure, the patient may wear a rigid head frame. Computed Tomography (CT) or Magnetic Resonance Imaging (MRI) help the doctor identify the tumor's exact location and a computer helps the doctor regulate the dose of radiation. Stereotactic radiotherapy is similar physically to radiosurgery but involves fractionation (multiple treatments). This modality would be recommended for tumors within or close to critical structures in the brain that cannot tolerate a large single dose of radiation or for larger tumors. This paper, propose three principledapproaches to compute the prescription dose. First, weminimize the surviving fraction of tumor cells after irradiationfor the most probable tumor cell density. Second, we minimizethe expected survival fraction tumor cells after irradiation.Third, we present an approach to correct the prescription doseto take into account the presence of adjacent organs at risk.The computed probability distribution over tumor cell densities, together with the cell survival model, is used to define the prescriptiondose distribution, which is the basis forsubsequent Intensity Modulated Radiation Therapy (IMRT) planning.Depending on the clinical data available first, we include the uncertainty in the segmentation process. We show how our method allows the user to compute a patient specific radiotherapy planning conformal to the tumor growth. The presented approach and its proof of concept may help in the future to better target the tumor and spare organs at risk.

## II-RELATED WORK

In [1], K. Farahani et al., proposed the new set-up and results of the Multimodal Brain Tumor Image Segmentation Benchmark (BRATS) organized in conjunction with the MICCAI 2012 and 2013 conferences. Quantitative evaluations revealed considerable disagreement between the human raters in segmenting various tumor sub-regions (Dice scores in the range 74%–85%), illustrating the difficulty of this task. We found that different algorithms worked best for different sub-regions (reaching performance comparable to human inter-rater variability), but that no single algorithm ranked in the top for all sub-regions simultaneously.
J. Murray et al.,[2] proposed a mathematical model to describe the growth and invasion of glioma cells throughout an anatomically accurate virtual human brain as well as the effects of operation on these lesions.
Olivier Saut et al.,[4] construct a clinical-scale model of GBM whose predictions uncover a new pattern of recurrence in 11/70 bevacizumab-treated patients. The findings support an exception to the Folkman hypothesis: GBM grows in the absence of angiogenesis by a cycle of proliferation and brain invasion that expands necrosis. Furthermore, necrosis is positively correlated with brain invasion in 26 newly-diagnosed GBM.
J. Unkelbach, et al.,[5]propose to analyze the model with respect to implications for target volume definition and identifies its most critical components. A retrospective study involving 10 glioblastoma patients treated at our institution has been performed. To illustrate the main findings of the study, a detailed case study is presented for a glioblastoma located close to the falx.
H. Delingette et al.,[6] propose a novel method for estimating the full extent of the tumor infiltration starting from its visible mass in the patients' MR images. This estimation problem is a time independent problem where we do not have information about the temporal evolution of the pathology nor its initial conditions. Based on the reaction-diffusion models widely used in the literature, we derive a method to solve this extrapolation problem. Later, we use this formulation to tailor new tumor specific variable irradiation margins.

## III-POPOSED SYSTEM

This section elucidates the system design and methodology which concerns its ultimate design and the features of proposed system. The overall system design of the proposed method is illustrated in Figure.1. The proposed work start with the acquisition of brain MR images of abnormal cases. The preprocessing techniques will help to improve the brain image quality and adaptive tumor segmentation technique is useful to segment the brain tumor portion separately. Tumor growth model generation is based on the reaction-diffusion method.

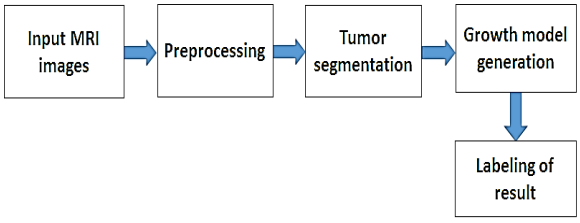


***Fig 1.Proposed block***

ISSN (Online) 2394-6849

International Journal of Engineering Research in Electronics and Communication Engineering (IJERECE)
Vol 4, Issue 12, December 2017

**A. Pre-processing techniques**

Brain MRIs are degraded during the process of imaging due to image transmission and image digitization by noise and existence of extra-cranial tissues in MRI such as Skull, bone, skin, air, muscles, and fat. Pre-processing is a procedure to eliminate these noises and extra-cranial tissues from the Brain MRI and alters the heterogeneous image into homogeneous image. Though there are lots of filters which have been used for filtering the images, some of them corrupt the miniature details of the image and some conventional filters will process the image incessantly (smoothing) and consequently harden the edges of the image. Hence, the proposed pre-processing steps namely De-noising and skull stripping provide better Image clarity.

**B. Contrast adjustment**

Contrast adjustment remaps image intensity values to the full display range of the data type. An image with good contrast has sharp differences between black and white.

The first step is to calculate a contrast correction factor which is given by the following formula:

$$F = \frac{259(C + 255)}{255(259 - C)}$$

In order for the algorithm to function correctly the value for the contrast correction factor (F) needs to be stored as a floating point number and not as an integer. The value C in the formula denotes the desired level of contrast.

The next step is to perform the actual contrast adjustment itself. The following formula shows the adjustment in contrast being made to the red component of a color:

$$R' = F(R - 128) + 128$$

This series and just ensures that the new values of red, green and blue are within the valid range of 0 to 255. The value of contrast will be in the range of -255 to +255. Negative values will decrease the amount of contrast and, conversely, positive values will increase the amount of contrast.

**C. Segmentation**

The T1Gd abnormality, which is the active part of the tumor, and the larger T2-FLAIR abnormality, which is usually called the edema, were segmented by a clinician. In order to take into account the uncertainty in the segmentation, we propose to randomly modify the original clinician segmentations. The method is based on, where samples of such segmentations are generated from a high dimensional Gaussian process, as the zero crossing of a level function. The samples are efficiently produced on the regular grid using the separability and stationary properties of the squared exponential covariance function. The samples take into account the image intensity information using the signed geodesic distance as the mean of the Gaussian process.

Segmentation samples for the T1Gd and T2-FLAIR abnormalities at the first and second time points are generated. Let S0 i denote the clinical segmentations for the T1Gd and T2- FLAIR abnormalities at the first and second time points, where the index i = 1,….,4 refers to the 4 available images. Let $S_i = \{S_i{}^k\}_{k=1,\dots K}$ denote sets of K plausible segmentations per modality and time point, where each $S_i{}^k$ is a plausible sample from $S_i{}^0$ , the ith clinician segmentation. The samples automatically respect the boundaries of the tumor progression such as the ventricles, because of the presence of large intensity gradients. The five presented samples per abnormality correspond to an average DICE of 87%, which is comparable to the inter-expert DICE measured in the BraTS Challenge for brain tumors delineation. Comparing the output of the forward tumor growth model with these plausible noisy segmentations allows to include the uncertainty of the original clinician segmentations. Note that other approaches could allow the handling of segmentation uncertainty. For instance, one could compare the output of the tumor growth model with probabilistic segmentation approaches which have been proposed for glioblastoma.

**D. Tumor Growth Model**

The tumor growth model is based on the reaction-diffusion equation,

$$\frac{\partial u}{\partial t} = \underbrace{\nabla(D.\nabla u)}_{\text{Diffusion}} + \underbrace{\rho u(1-u)}_{\text{Logistic Proliferation}} \quad \_(1)$$

$$D\nabla u.\vec{n}_{\partial\omega} \quad \_(2)$$

Equation (1) describes the spatio-temporal evolution of the tumor cell density u, which infiltrates neighboring tissues with a diffusion tensor D, and proliferates with a net proliferation rateρ. Equation (2) enforces Neumann boundary conditions on the brain domainω. Following, we define the diffusion tensor as D = dw I in the white matter, and D = dw/10 I in the gray matter, where I is the 3x3 identity matrix. Below, we identify the scalar parameter dw with D. The solution of the reaction-diffusion equation (1) is a tumor cell density u computed over the whole brain domain. However, parts of the brain that glioblastomas usually do not invade were excluded from the tumor simulation such as the CSF or the cerebellum. In order to relate the tumor cell density u to the MRIs, the frontier of the visible abnormalities is assumed to correspond to a threshold value of the tumor cell density u. We note $\tau_1$ the value of the tumor cell density u corresponding to the frontier of the T1Gd abnormality, and $\tau_2$ the value corresponding to the frontier of the T2-FLAIR abnormality. The initialization of the tumor cell density u (t = t1, x) at the time of the first acquisition is of particular importance, as it impacts the rest of the simulation. In this work, the tumor tail extrapolation algorithm described. The method is based on the assumption that the solution of equation (1) at the

ISSN (Online) 2394-6849

International Journal of Engineering Research in Electronics and Communication Engineering (IJERECE)
Vol 4, Issue 12, December 2017

first time point has converged to its asymptotic, traveling wave type solution. Thereby, the tumor cell density is propagated outward (and inward), starting from the T1Gd segmentation, and drops approximately exponentially with distance. The steepness of the falloff, i.e. the distance at which the cell density drops by a factor 1/e is given by the invisibility index $\lambda = \sqrt{D/\rho}$. By construction of the initialization, the T1Gd abnormality falls exactly on the threshold $\tau_1$ of the tumor cell density at the first time point. The reaction-diffusion equation is solved using the Lattice Boltzmann Method which allows for easy parallelization and fast computations. On a 1mm x 1mm x 1mm resampled MRI, simulating 30 days of growth takes approximately 50 seconds on a 2.3 GHz 50 core machine. Note that this model is an approximation of the complex growth of the disease. For instance, it could be extended in order to include mass effect, or a more detailed description of the disease. In other works, this model has been extended to model different types of therapy such as resection, chemotherapy, or anti-angiogenic therapy. The common approach taken in these works is to add a death term to the reaction-diffusion equation, which allows to model the shrinkage of the tumor due to the therapy. The personalized parameters of a reaction-diffusion model were good predictors of certain mutations status of the patient.

## IV - SIMULATION RESULTS

The Brain MRI images area collected from the 'prostatemrimage' database and the different stages of the MRI images of a single patient is collected and tested in this work. The following figure 1 and represents the test images sample images. Where the figure 1 is starting stages of the brain tumor and the figure 2 represents the prostate stage of the brain tumor.

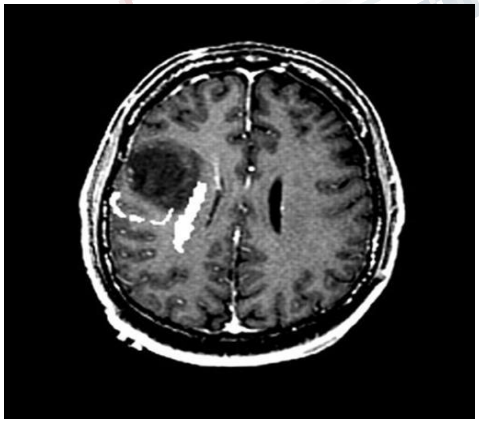

***Figure 1 sample test image with initial brain tumor***

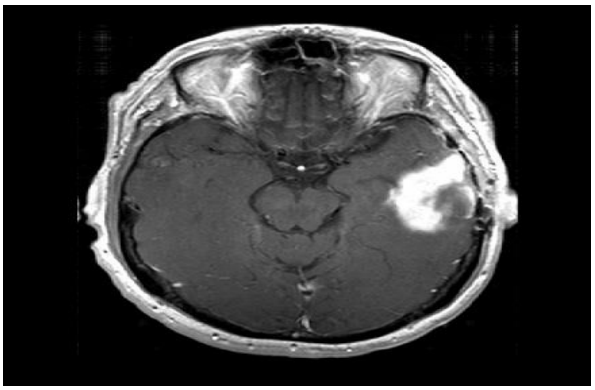

***Figure 2 sample test image with prostate brain tumor***

The following figure represents the 8 stages of the brain tumor MRI images.

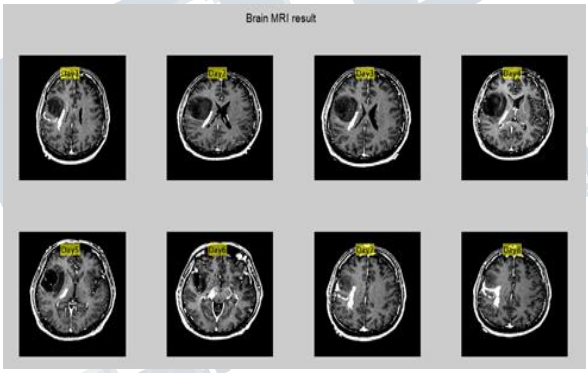


***Figure 3 Eight stages of brain tumor***

The preprocessing and segmentation is taken for the tumor region and the following figure is showing the eight different stages of the brain tumor images, the tumor regions are represented with the help of binary images. The tumor image is indicated by the white pixels and the background pixels are represented as black.

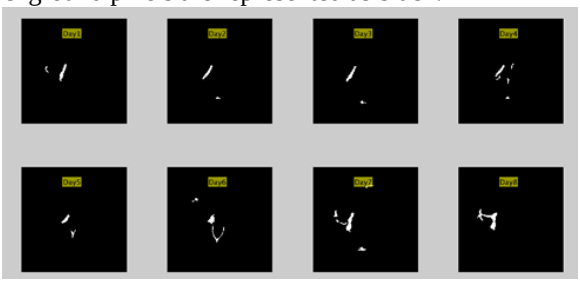

***Figure 4 segmented tumor ROI of brain tumor***

The labeling of the segmented region is most helpful for the radiotherapy implementation and the dosage can be planned based in the labeling on the original images.

ISSN (Online) 2394-6849

International Journal of Engineering Research in Electronics and Communication Engineering (IJERECE)
Vol 4, Issue 12, December 2017

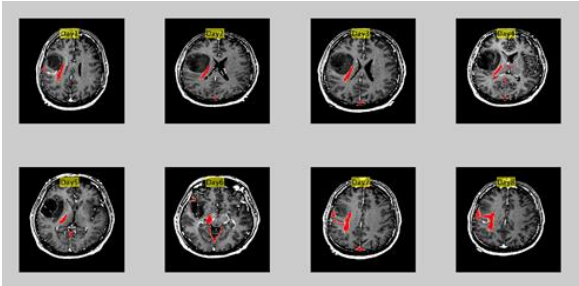

*Figure 5 labeled tumor ROI of brain tumor*

The area of the tumor region is calculated based o the morphological operations and the pixels count is the actual area of the tumor ROI. The area measurement are converted form the pixel units into millimeter units. And the following figure is showing the Area representation of the different stages of the Brain tumor ROI.

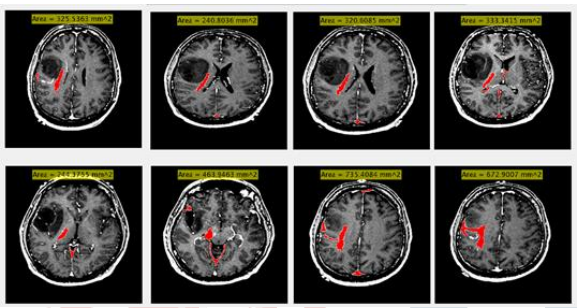

*Figure 4 area representation of brain tumor*

| Day | Area in (mm^2) | Growth model |
|---|---|---|
| Day1 | 325.54 | Initial |
| Day2 | 240.80 | decrease |
| Day3 | 320.61 | increase |
| Day4 | 333.34 | increase |
| Day5 | 244.38 | decrease |
| Day6 | 463.95 | increase |
| Day7 | 735.41 | increase |
| Day8 | 672.90 | decrease |

**(i) Performance Evaluation**

This section delivers the performance of the grade classification work where the proposed work has classified the test samples with two classifiers called SVM and KNN classifiers

**(a) Accuracy**

Accuracy is the degree to which the result of a measurement, calculation, or specification conforms to the correct value or a standard

$$\text{Accuracy} = \frac{TP+FN}{TP+TN+FP+FN}$$

The proposed work is achieving the maximum accuracy level as 98.91% and also obtaining the maximum recognition rate for this deep learning based work. Performance measure procedure was done by comparing the segmentation results to the reference image. There are four values resulted from the validation procedure, True Positive (TP), False Positive (FP), True Negative (TN) and False Negative (FN). True Positives is a number of images correctly detected as normal, False Positive is a number of images incorrectly detected True Negatives is a number of images correctly detected as tumor image and False Negative (FN) is a number of image incorrectly detected as tumor.

***Table.1: Target vs predicted***

| Target vs Predicted | Normal pixel (Predicted) | Tumorous pixel (Predicted) |
|---|---|---|
| Normal pixel (Target) | True positive (TP) | False positive (FP) |
| Tumorous pixel (Target) | False Negative (FN) | True Negative (TN) |

For evaluation purpose, all the parameters are determined for each image in the dataset. Sensitivity, Specificity and Predictivity, Recall, True Positive Rate, False Positive Rate are used as performance measures.

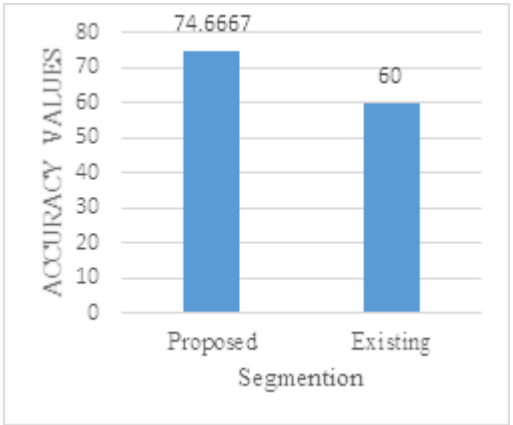


***Fig 5. Accuracy graph***

ISSN (Online) 2394-6849

International Journal of Engineering Research in Electronics and Communication Engineering (IJERECE)
Vol 4, Issue 12, December 2017

**(b) Sensitivity**

Sensitivity is the probability that a test result will be positive when the selected pixel is normal. It is defined as the ratio between True positive (TP) and addition of True positive (TP) and False negative (FN).

$$\text{Sensitivity} = \frac{TP}{TP+FN}$$

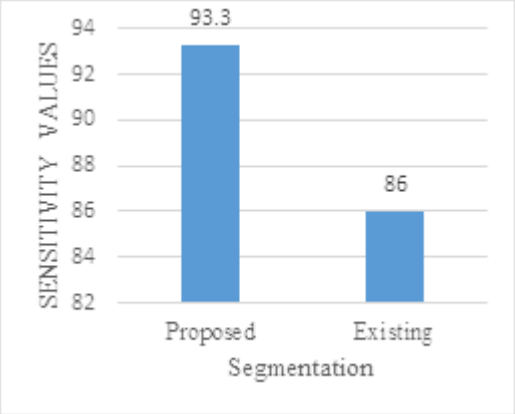


***Fig 6. Sensitivity graph***

## V. CONCLUSION

The proposed work is delivering the brain tumor growth model generation based on the tumor intensity based approach. The first step in this work is based on the tumor region segmentation. The segmented brain tumor region is undergone for the area measurement. The area measurement is done with the help of morphological operation and the successive images are undergone for the same fashion of area measurement. The brain tumor growth model is predicted for the sequence of MRI images. This work is accurately targeting the tumor region and it will be helpful for the further growth model. The proposed work is developed in MATLAB environment.

## REFERENCES

[1] B. Menze, A. Jakab, S. Bauer, J. Kalpathy-Cramer, K. Farahaniet al., "The multimodal brain tumor image segmentation benchmark(BRATS)," Medical Imaging, IEEE Transactions on, vol. 34, no. 10,pp. 1993–2024, 2015.

[2] K. Swanson, E. Alvord, and J. Murray, "Virtual resection of gliomas:effect of extent of resection on recurrence," Mathematical and ComputerModelling, vol. 37, no. 11, pp. 1177–1190, 2003.

[3] R. Rockne, E. Alvord Jr, J. Rockhill, and K. Swanson, "A mathematical model for brain tumor response to radiation therapy," Journal of mathematical biology, vol. 58, no. 4-5, pp. 561–578, 2009.

[4] E. Scribner, O. Saut, P. Province, A. Bag, T. Colin, and H. M.Fathallah-Shaykh, "Effects of anti-angiogenesis on glioblastoma growthand migration: model to clinical predictions," PloS one, vol. 9, no. 12,p. e115018, 2014.

[5] J. Unkelbach, B. H. Menze, E. Konukoglu, F. Dittmann, N. Ayache, andH. A. Shih, "Radiotherapy planning for glioblastoma based on a tumorgrowth model: implications for spatial dose redistribution," Physics inmedicine and biology, vol. 59, no. 3, p. 771, 2014.

[6] E. Konukoglu, O. Clatz, P.-Y. Bondiau, H. Delingette, and N. Ayache,"Extrapolating glioma invasion margin in brain magnetic resonanceimages: Suggesting new irradiation margins," Medical image analysis,vol. 14, no. 2, pp. 111–125, 2010.

[7] O. Saut, J.-B. Lagaert, T. Colin, and H. M. Fathallah-Shaykh, "A multilayer grow-or-go model for gbm: effects of invasive cells and anti-angiogenesis on growth," Bulletin of mathematical biology, vol. 76, no. 9, pp. 2306–2333, 2014.

[8] F. Raman, E. Scribner, O. Saut, C. Wenger, T. Colin, and H. M. Fathallah-Shaykh, "Computational trials: Unraveling motility phenotypes, progression patterns, and treatment options for glioblastomamultiforme," PloS one, vol. 11, no. 1, 2016.

[9] K. Kristiansen, S. Hagen, T. Kollevold, A. Torvik, I. Holme, M. Stat, R. Nesbakken, R. Hatlevoll, M. Lindgren, A. Brun et al., "Combined modality therapy of operated astrocytomas grade III and IV. Confirmation of the value of postoperative irradiation and lack of potentiation of bleomycin on survival time: a prospective multicenter trial of the Scandinavian Glioblastoma Study Group," Cancer, vol. 47, no. 4, pp. 649–652, 1981.

[10] I. J. Barani and D. A. Larson, "Radiation therapy of glioblastoma," in Current Understanding and Treatment of Gliomas. Springer, 2015, pp. 49–73.